

ExoMol molecular line lists – XXIII. Spectra of PO and PS

Laxmi Prajapat,¹ Pawel Jagoda,¹ Lorenzo Lodi,¹ Maire N. Gorman,^{1,2}
Sergei N. Yurchenko¹★ and Jonathan Tennyson¹★

¹Department of Physics and Astronomy, University College London, London WC1E 6BT, UK

²Department of Physics, Aberystwyth University, Penlais, Aberystwyth, Ceredigion SY23 3BZ, UK

Accepted 2017 August 25. Received 2017 August 19; in original form 2017 July 18

ABSTRACT

Comprehensive line lists for phosphorus monoxide ($^{31}\text{P}^{16}\text{O}$) and phosphorus monosulphide ($^{31}\text{P}^{32}\text{S}$) in their $X^2\Pi$ electronic ground state are presented. The line lists are based on new *ab initio* potential energy (PEC), spin-orbit (SOC) and dipole moment (DMC) curves computed using the MRCI+Q-r method with aug-cc-pwCV5Z and aug-cc-pV5Z basis sets. The nuclear motion equations (i.e. the rovibronic Schrödinger equations for each molecule) are solved using the program DUO. The PECs and SOCs are refined in least-squares fits to available experimental data. Partition functions, $Q(T)$, are computed up to $T = 5000$ K, the range of validity of the line lists. These line lists are the most comprehensive available for either molecule. The characteristically sharp peak of the Q -branches from the spin-orbit split components gives useful diagnostics for both PO and PS in spectra at infrared wavelengths. These line lists should prove useful for analysing observations and setting up models of environments such as brown dwarfs, low-mass stars, O-rich circumstellar regions and potentially for exoplanetary retrievals. Since PS is yet to be detected in space, the role of the two lowest excited electronic states ($a^4\Pi$ and $B^2\Pi$) are also considered. An approximate line list for the PS X - B electronic transition, which predicts a number of sharp vibrational bands in the near ultraviolet, is also presented. The line lists are available from the CDS (<http://cdsarc.u-strasbg.fr>) and ExoMol (www.exomol.com) data bases.

Key words: molecular data – opacity – astronomical data bases: miscellaneous – planets and satellites: atmospheres – stars: AGB and post-AGB – stars: atmospheres.

1 INTRODUCTION

Several phosphorus-containing molecules have been discovered around evolved stars including PN, HCP, CP and PO (Tenenbaum, Woolf & Ziurys 2007; Milam et al. 2008; De Beck et al. 2013) and PH_3 has been detected in the circumstellar envelope of IRC+10216 (Agundez et al. 2014). Other phosphorous-containing species including PS are yet to be detected (De Beck et al. 2013). Models suggest that a variety of phosphorous-bearing species become important in the atmospheres of low-mass stars, brown dwarfs and giant exoplanets at elevated temperatures (Visscher, Lodders & Fegley 2006). PN has been observed in the 3 mm region towards the low-mass star-forming region of L1157 (Yamaguchi et al. 2011, 2012).

Additionally, being a primal biogenic element found in all living systems, phosphorus is hence essential to life on Earth (Maciá, Hernández & Oró 1997). Phosphorus is present in nucleic acids, several proteins, and is a fundamental component of the adenosine triphosphate molecule, which is accountable for energy transfer in cells. P-containing molecules are thought to provide important biomarkers in the early Earth (Li, Sun & Chan 2013)

and such molecules could play a similar role in exoplanets. In addition, the atmospheres of the recently characterized hot rocky planets, or lava planets, are likely to contain a whole range of unusual small molecules (Tennyson & Yurchenko 2017). In this work, performed as part of the ExoMol project (Tennyson & Yurchenko 2012), we concentrate on providing comprehensive line lists for the two open shell diatomic species: PO and PS. Oxygen and sulphur belong to the same group in the periodic table and, as a result, PO and PS have similar electronic structures (e.g. both have a $X^2\Pi$ ground electronic state) and their spectra show many analogies.

After a number of failed attempts (Matthews, Feldman & Bernath 1987; Dimur et al. 2001; MacKay & Charnley 2001), phosphorus monoxide, PO, has been detected in a number of locations in space. The original detection, by Tenenbaum et al. (2007), was in the oxygen-rich, red Supergiant Star VY Canis Majoris and used microwave emissions near 240 and 284 GHz (7.2 and 8.5 cm^{-1}). Subsequently PO has been observed in the wind of the oxygen-rich AGB star IK Tauri (De Beck et al. 2013) and in star-forming regions (Lefloch et al. 2016; Rivilla et al. 2016). In a number of these locations, PO appears to occur with similar abundance to the closed shell molecule PN for which an ExoMol line list has already been constructed (Yorke et al. 2014).

* E-mail: s.yurchenko@ucl.ac.uk (SNY); j.tennyson@ucl.ac.uk (JT)

As of yet there are no observations of phosphorus monosulphide, PS, in space (De Beck et al. 2013). A systematic attempt at its astronomical detection was performed by Ohishi et al. (1988) using the 45m telescope of the Nobeyama Radio Observatory and six distinct objects. Local thermodynamic equilibrium calculations by Tsuji (1973) indicate that PS should be the major P-bearing molecule in oxygen-rich circumstellar envelopes for temperatures below 2000 K.

Available line lists for both PO and PS appear to be extremely limited. Long-wavelength transition frequencies are available for both species in the JPL data base (Pickett et al. 1998), but the transition intensities are all based on assumed or estimated values for the permanent dipole moments. A more up-to-date long-wavelength line list for PO is given by the Cologne Database for Molecular Spectroscopy (CDMS) (Müller et al. 2005).

There have been several studies that aimed to obtain line frequencies and spectroscopic constants of PO from experimental and theoretical analyses of its spectrum (Ghosh & Verma 1978; Rao, Reddy & Rao 1981; Butler, Kawaguchi & Hirota 1983; Kanata, Yamamoto & Saito 1988; Qian 1995; de Brouckere 1999; Spielfiedel & Handy 1999; Bailleux et al. 2002; Metropoulos, Papakondylis & Mavridis 2003; Moussaoui, Ouamerali & De Mare 2003; Sun, Wang & Shi 2012; Liu et al. 2013). A review of the experimental work on PO prior to 1999 is given by de Brouckere (1999), while Liu et al. (2013) provide a more recent summary of *ab initio* studies. In addition to work on the spectrum of PO in its $X^2\Pi$ ground electronic state, there have also been extensive experimental studies of its excited electronic states. Early work on observed transitions is summarized by Huber & Herzberg (1979); Huber and Herzberg list in their compilation for PO 13 electronic states up to about $56\,000\text{ cm}^{-1}$ (six $^2\Sigma^+$ states, one $^2\Sigma^-$ state, three $^2\Pi$ states, two $^2\Delta$ state and one $^4\Sigma^-$ state). Additional excited electronic states, including more quartet and sextet states, have been considered theoretically (Kanata et al. 1988; de Brouckere 1999, 2000; Spielfiedel & Handy 1999; Metropoulos et al. 2003; Moussaoui et al. 2003; Sun et al. 2012; Liu et al. 2013).

PS was observed in the laboratory for the first time by Dressler & Miescher (1955) who detected two band systems corresponding to the $C^2\Sigma \rightarrow X^2\Pi$ and $B^2\Pi \rightarrow X^2\Pi$ electronic transitions, with wavelength ranges 2700–3100 and 4200–6000 Å, respectively. Since then a limited set of experiments on PS have followed (Narasimham & Subramanian 1969; Narasimham & Balasubramanian 1971; Jenouvrier & Pascat 1978; Balasubramanian, Dixit & Narasimham 1979; Lin, Balling & Wright 1987; Kawaguchi et al. 1988; Ohishi et al. 1988; Wang et al. 1993) with the most recent being the study of a submillimetre-wave rotational spectrum by Klein, Klisch & Winnewisser (1999). Several of these studies are considered further below. There have also been various theoretical studies conducted on the ground and electronic states of PS (Bruna & Grein 1987; Karna, Bruna & Grein 1988; Karna & Grein 1992; Moussaoui, Ouamerali & De Mare 1998; Kalcher 2002; Ben Yaghlane, Francisco & Hochlaf 2012), including a Multi-Reference Configuration Interaction (MRCI) study of the lowest 16 molecular terms by Ben Yaghlane et al. (2012).

The aim of this work is to produce molecular line lists for $^{31}\text{P}^{16}\text{O}$ and $^{31}\text{P}^{32}\text{S}$ applicable for a large range of temperatures.

2 METHOD

In the theoretical approach adopted by our group (Lodi & Tennyson 2010) the computation of a line list for the molecule of interest requires constructing potential energy curves (PECs),

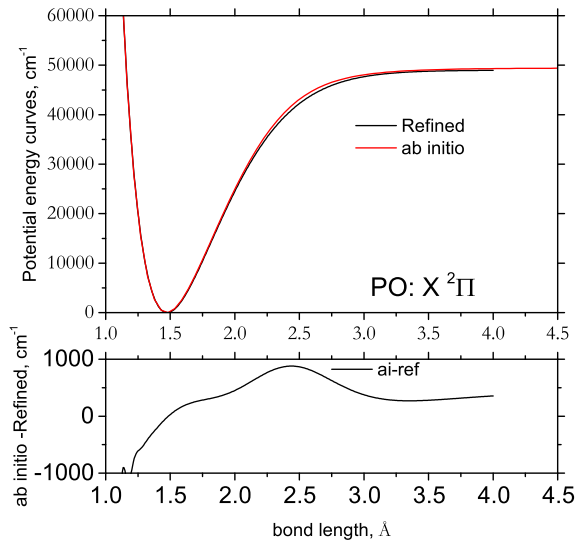


Figure 1. Comparison of *ab initio* (MRCI+Q-r/aug-cc-pwCV5Z) and refined PECs of PO.

dipole moment curves (DMCs), spin-orbit couplings (SOCs) and, if necessary, other couplings such as angular momentum, spin-spin and spin-rotation (Tennyson et al. 2016b). These are then used to solve the relative nuclear motion Schrödinger equation, thus producing frequencies and intensities for the transitions of interest.

2.1 *Ab initio* electronic structure data

2.1.1 PO

While there have been several *ab initio* studies of PO's many electronic states which yielded total energies and spectroscopic constants, none of them supply the PECs, SOC and DMCs required for the construction of a line list. *Ab initio* curves were therefore computed using MOLPRO (Werner et al. 2012). The chosen technique was MRCI+Q-r (internally contracted multireference configuration interaction with renormalized Davidson correction; the 'relaxed reference' energy was used) with the aug-cc-wCV5Z basis set. The calculation also included a relativistic correction curve computed as the expectation value of the mass-velocity plus one-electron Darwin operator (MVD1). The *ab initio* PEC was computed up to a nuclear separation of 4.5 Å and can be seen in Fig. 1.

The *ab initio* SOC was obtained using the same level of theory. Fig. 2 shows the *ab initio* SO curve, as well as the refined curve (see below). The equilibrium *ab initio* SO value (106.4 cm^{-1}) is in reasonable agreement with the empirical SO constant ($A_{\text{SO}}/2 = 112.1\text{ cm}^{-1}$) from Butler et al. (1983) and with the *ab initio* value 112.6 cm^{-1} of Liu et al. (2013). Our refined equilibrium SO value is 112.1 cm^{-1} .

Our value of the equilibrium bond length $r_e = 1.482\text{ Å}$ obtained from the PEC of the $X^2\Pi$ state is in reasonable agreement with the most recent experimentally determined value $r_e = 1.475\,637\,355(10)\text{ Å}$ (Bailleux et al. 2002). The dissociation value $D_e = 48\,997.9\text{ cm}^{-1}$ also compares well with the value $48\,980\text{ cm}^{-1}$ (6.073 eV) estimated by Rao et al. (1981). This *ab initio* PEC thus provides a suitable starting point for empirical refinement of the $X^2\Pi$ state.

At the start of this work there was no DMC for the $X^2\Pi$ state of PO available in the literature with instead the majority of *ab initio*

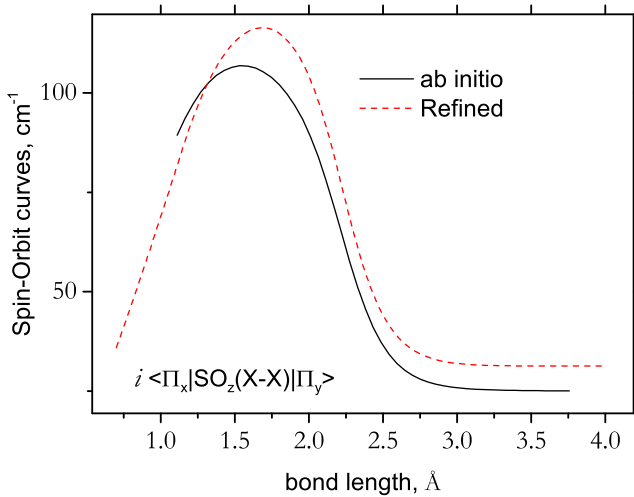


Figure 2. Comparison of PO spin-orbit curves. Solid line: *ab initio* curve; red dashed line: empirical curve produced using the morphing approach.

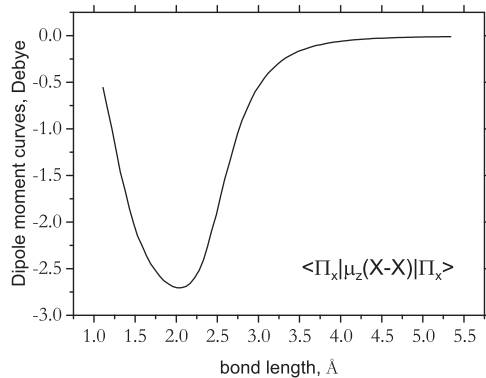


Figure 3. *Ab initio* DMC for the ground state of PO.

studies focusing on the myriad of low-lying PECs of PO. Moussaoui et al. (2003) computed a value for the dipole at equilibrium and recently Andreatza, de Almeida & Borin (2016) computed curves as part of their study on the formation of PO by radiative association.

The experimental data are limited to the μ_0 value by Rao et al. (1981). Therefore, it was decided to use the highest level of *ab initio* theory in this work to produce a suitable DMC for the line list calculation. Similar to the final *ab initio* PEC, the *ab initio* DMC was calculated using the MRCI+Q-r/aug-cc-pwCV5Z; it was calculated as the derivative of the MRCI+Q-r energy with respect to an external electric field along the internuclear axis for vanishing field strength (Lodi & Tennyson 2010).

The dipole moment generated for the $X^2\Pi$ state of PO is shown in Fig. 3. Its value at the equilibrium bond length is 1.998 D, which is in reasonable agreement with 1.88 ± 0.07 D (Kanata et al. 1988) (also adopted by CDMS; Müller et al. 2005) and therefore provides an adequate choice in the final calculation of the line list. These values are much larger than the value of 1.0 D assumed in the JPL line list (Pickett et al. 1998).

2.1.2 PS

Ab initio curves for the ground ($X^2\Pi$) and three excited ($a^4\Pi$, $B^2\Pi$ and $4^2\Sigma^-$) electronic states of PS were generated using MOLPRO and the MRCI+Q-r method with the aug-cc-pwCV5Z basis sets used

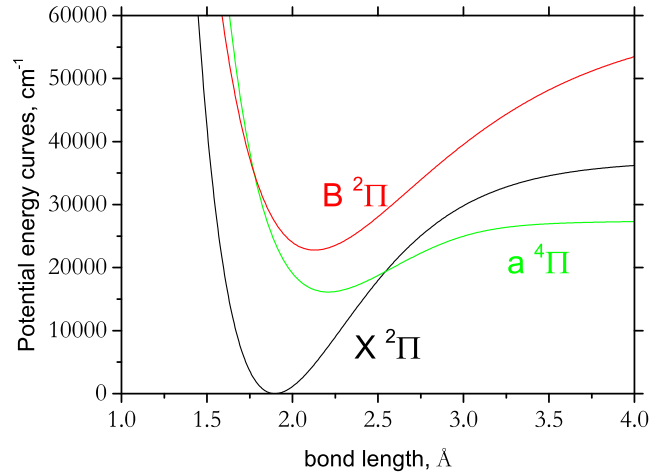


Figure 4. Refined PECs for the $X^2\Pi$, $B^2\Pi$ electronic states and the *ab initio* PEC for the $a^4\Pi$ electronic state of PS.

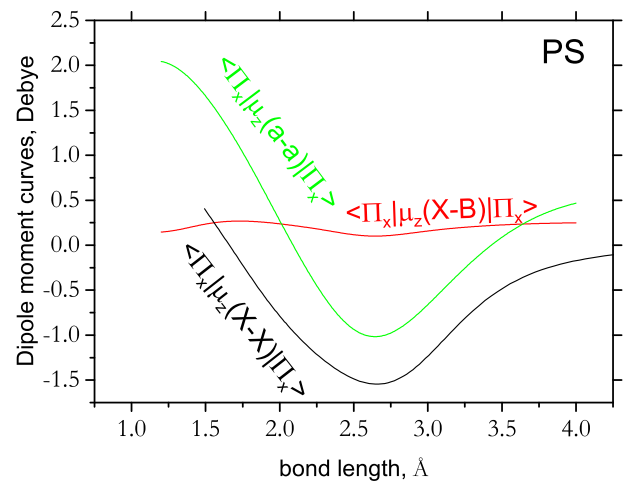


Figure 5. *Ab initio* DMCs of PS which were represented analytically.

for the ground state and aug-cc-pV5Z basis sets used for the excited states. The *ab initio* PEC of the $a^4\Pi$ state and the refined PECs for the $X^2\Pi$ and $B^2\Pi$ states considered in this paper are shown in Fig. 4. The dissociation limit obtained by our calculation for the $X^2\Pi$ electronic state appears to be close to the estimated $D_e = 36\,600$ cm^{-1} (438 ± 10 kJ mol^{-1}) of Drowart et al. (1973), although we did not perform calculation at large enough bond lengths to quote an accurate value. Our equilibrium dipole moment of the X state is 0.523 D, which can be compared to the complete basis set extrapolation value by Muller & Woon (2013) of 0.565 D.

The *ab initio* DMCs for the ground $X^2\Pi$ electronic state, excited $a^4\Pi$ electronic state and for the $X^2\Pi$ – $B^2\Pi$ electronic transition considered in this work for PS are shown in Fig. 5. In order to reduce the numerical noise when computing the line-strengths using the DUO program, we followed the recommendation of Medvedev et al. (2016) and represented analytically the *ab initio* DMCs (denoted by $\mu(r)$). The following expansion with a damped-coordinate was employed:

$$\mu(r) = (1 - \xi) \sum_{n \geq 0} d_n z^n + d_\infty \xi, \quad (1)$$

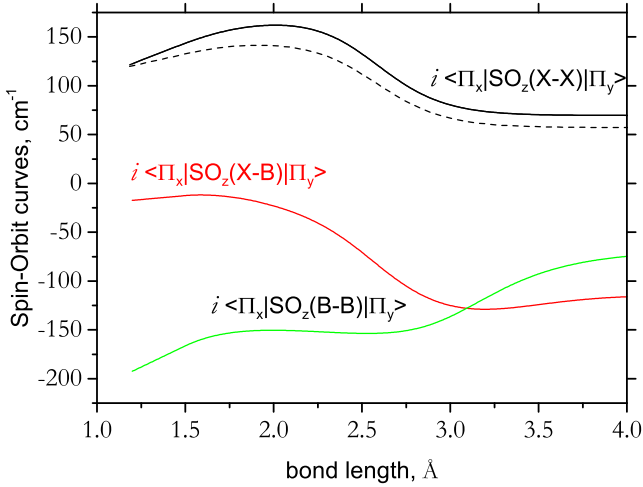


Figure 6. Spin–orbit curves of PS, *ab initio* (solid) and refined (dashed).

where ξ is the Šurkus variable (Šurkus, Rakauskas & Bolotin 1984)

$$\xi = \frac{r^p - r_{\text{ref}}^p}{r^p + r_{\text{ref}}^p} \quad (2)$$

and z is given by

$$z = (r - r_{\text{ref}}) e^{-\beta_2(r-r_{\text{ref}})^2 - \beta_4(r-r_{\text{ref}})^4}.$$

Here p is an empirical parameter, r_{ref} is a reference position equal to r_e by default, d_n are the expansion parameters, d_∞ is the value of the dipole at $r \rightarrow \infty$, and β_2 and β_4 are damping factors. These parameters defining the dipole moment expansion for the three *ab initio* DMCs considered in this work for PS are given in the supplementary material as a DUO input file, while the functional form is now a part of the DUO program.

The SOCs were computed using the aug-cc-pVDZ basis set (valence only calculations) to speed up their calculation [SOCs are not expected to be very sensitive to the level of theory used, see Patrascu et al. (2014)] and are shown in Fig. 6. Our equilibrium SO *ab initio* value is 141.4 cm⁻¹ and after refinement is 160.9 cm⁻¹. The analogous experimental effective SO constant $A_{\text{SO}}/2$ was determined to be 161.0 cm⁻¹ by Jenouvrier & Pascat (1978).

2.2 Nuclear motion calculations

The nuclear motion calculations were performed using the code DUO (Yurchenko et al. 2016), which provides a variational solution to the nuclear motion problem and can account for virtually any coupling between the PECs of the molecule under study. A review of the theory on which DUO is based can be found in Tennyson et al. (2016b). The necessary curves can be computed using *ab initio* electronic methods or by fitting to experimental data. Our general strategy (Tennyson 2012; Tennyson & Yurchenko 2017), which is followed here, is to use spectroscopically determined PECs and couplings, since these cannot be computed with sufficient accuracy by *ab initio*

methods (McKemmish, Yurchenko & Tennyson 2016). Conversely, experience has shown that *ab initio* DMCs give results that are very reliable (Tennyson 2014) and can give intensities that are competitive in accuracy with the most precise laboratory measurements (Polyansky et al. 2015). In general, the nuclear motion problem can be solved with sufficient accuracy that the quality of the underlying *ab initio* curves is the main source of error in the calculations.

2.3 Refinement using experimental data

2.3.1 PO

Table 1 lists the sources used in refining the PO $X^2\Pi$ PEC. Most of the 241 lines used correspond to pure rotational transitions observed in microwave and far-infrared studies, including hot bands $\Delta v = 0$ and $v' \leq 7$. The only source of IR data is the laser spectroscopy study by Qian (1995) where 50 fundamental transitions ($J \leq 21.5$) were reported. Butler et al. (1983) and Bailleux et al. (2002) resolved the hyperfine structure within each observed rotational transition. As hyperfine splitting is beyond the scope of this work, frequencies resulting from such transitions were averaged over for each rotational transition.

We also included lower accuracy experimentally derived vibrational energies by Verma & Singhal (1975) with T_v with $v \leq 11$. The availability of these vibrational terms values provided an important constraint for extrapolation of vibrational levels higher than $v = 1$.

It is easier to start the DUO refinement by fitting to energies, not transition frequencies. To this end, an ‘experimentally derived’ set of energy levels of PO was produced using the program PGO-PHER (Western 2017) in conjunction with the experimentally derived spectroscopic constants for the ground ($v = 0$) and first excited ($v = 1$) vibrational states, as determined in Qian (1995). These energies (up to $J = 26.5$) were combined with the vibrational energies by Verma & Singhal (1975).

2.3.2 PS

There is little laboratory data available on the $X^2\Pi$ state of PS. Dressler & Miescher (1955), Narasimham & Subramanian (1969), Narasimham & Balasubramanian (1971) and Balasubramanian et al. (1979) reported vibronic heads only and did not provide any information that can be used to refine this state. Kawaguchi et al. (1988), Ohishi et al. (1988) and Klein et al. (1999) give millimetre wave spectra that provide information on the rotational levels and spin-orbit splitting between the states. Ohishi et al. (1988) and Klein et al. (1999) provide hyperfine-resolved transition frequencies that were unresolved by averaging the frequencies of matching transitions with the same ef , J' , J'' and Ω values, where Ω is the projection of the total angular momentum. The ef parity was not provided for $\Omega = \frac{3}{2}$ in Ohishi et al. (1988) and Kawaguchi et al. (1988); it was assumed to be unresolved and were duplicated for later use. Kawaguchi et al. (1988) provides data on the vibrational fundamental. In addition, we used the program PGO-PHER to derive a set

Table 1. Experimental sources used in the empirical refinement of the PO PEC.

Source	Method	Transitions	lines	Range (cm ⁻¹)	Uncertainty (cm ⁻¹)
Bailleux et al. (2002)	Millimetre wave	$\Delta v = 0, v = 0 : 7, J \leq 10.5$	167	4.98–15.39	0.01
Qian (1995)	Microwave, IR	$v = 1 \leftarrow 0, J \leq 21.5$,	46	1188.12–1245.12	0.0005
Butler et al. (1983)	Mid-IR	$\Delta v = 1, v = 0 - 1, J \leq 25.5$,	28	2.1226–1254	0.0005
Verma & Singhal (1975)	UV	T_v for $v = 0 : 11$		$E_v = 0 - 12\,700.05$	0.02

of PS energy levels from the spectroscopic constants reported in the experimental paper by Klein et al. (1999). This gave a total of 316 energies for J ranging from 0.5 to 39.5 split between the $\nu = 0$ and $\nu = 1$ state. For the vibrationally excited states, we added the vibrational energies reconstructed from the vibrational $\Delta\nu = 1$ separations reported by Jenouvrier & Pascat (1978) from analysis of the $B^2\Pi-X^2\Pi$ system. The energies coincided with consecutive vibrational transitions from $\nu = 0$ to 9.

To make all data internally consistent, the experimental e/f parities for the lower state were converted into the $+/-$ parities (Brown et al. 1975) using the standard relations:

$$e : (-1)^{J-\frac{1}{2}} \quad (3)$$

and

$$f : (-1)^{J+\frac{1}{2}}. \quad (4)$$

The selection rule $+\leftrightarrow-$ was used to determine the parity for the upper state. The frequency and quantum numbers were repeated for both $+$ and $-$ whenever the parities were unavailable in the experimental data (all in the case of the $^2\Pi_{\frac{3}{2}}$ sub-state). Σ' and Σ'' values (projections of the electronic spin on the molecular axis) were derived from $|\Omega|$ usually provided in experimental literature as $|\Omega| = |\Lambda \pm \Sigma'|$ and by matching the corresponding parity. Here $\Lambda = \pm 1$ is the projection of the electronic angular momentum and Ω is the projection of the total angular momentum on the molecular axis.

2.4 Fitting with DUO

DUO offers a range of analytical functions for modelling PECs. Owing to its previous success in producing accurate PECs, it was decided to use the Extended Morse Oscillator (EMO) function (Lee et al. 1999) to obtain the final $X^2\Pi$ PECs for PO and PS denoted by $V(r)$. The function is written

$$V(r) = D_e \left[1 - \exp \left(- \sum_{k=0}^N \beta_k \xi^k (r - r_e) \right) \right]^2, \quad (5)$$

where ξ is the Šurkus variable, see equation (2). Here β_k is an empirical parameter whose value (along with the parameter p) can be derived through refinement to experimental data. It is important to note that $V(+\infty) = D_e$, as long as both p and $\sum_k \beta_k$ are set greater than zero.

DUO also allows the SOC to be refined simultaneously with the PEC. An *ab initio* curve $F_{\text{ai}}(r)$ can be scaled using the morphing approach so that the empirical curve, $F(r)$, is given by

$$F(r) = H(r)F_{\text{ai}}(r) \quad (6)$$

with

$$H(r) = \left[(1 - \xi) \sum_{k=0}^N \beta_k \xi^k + \xi t_\infty \right], \quad (7)$$

where $H(r)$ is the morphing function in terms of the Šurkus variable (ξ), t_∞ is the value of the morphing function as $r \rightarrow \infty$ and β_k is the morphing expansion coefficient (Yurchenko et al. 2016). The morphing approach was used to refine the *ab initio* SOC. As there were no available *ab initio* curves for spin-rotation (SR) and Λ -doubling effects, the functional form $H(r)$ was applied to both couplings directly.

The final DUO input files for both PO and PS are given as part of the supplementary material. These files contain the various curves as well as the parameters used to run DUO.

2.4.1 PO

Experimental values of PO for dissociation D_e (Rao et al. 1981) and equilibrium bond length r_e (Baillieux et al. 2002) were held fixed until the final stages of the refinement process. The first four β_k expansion coefficients from equation (5) were varied by fitting to experimentally derived energies of PO obtained using PGOPHER until a satisfactory fit was achieved. At this point the empirical energies were replaced by the actual, measured frequencies for comparison and further refinement. As the reference frequencies only include pure rotational and fundamental absorption lines, to increase constraints on the higher vibrational transitions, the differences between the higher vibrational energies (Verma & Singhal 1975) relative to the ground level ($\nu = 0$) were retained.

At the final stage of refinement, two additional terms were introduced to account for spin-rotation and any additional Λ -doubling effects to further minimize Obs. – Calc. The resulting empirical PEC and SOC are shown in Figs 1 and 2, respectively: these are plotted with the respective *ab initio* curves for comparison. The final parameters as well as the corresponding curves are given as part of the DUO input files in supplementary data.

The accuracy of the fit ranges from 0.001 cm^{-1} for purely rotational transitions up to 0.05 cm^{-1} for vibrational transitions, producing a root mean square (RMS) error of 0.014 cm^{-1} . The residuals are illustrated in Fig. 7, where the vibronic bands are indicated. Table 2 illustrates the Obs. – Calc. residuals for the vibrational excitations of PO and PS. In both cases the empirical term values are of limited accuracy (Verma & Singhal 1975; Jenouvrier & Pascat 1978), especially for the PS values from Jenouvrier & Pascat (1978). While the target accuracy of the PEC was achieved for low vibrational levels, having access to more experimental data for higher levels would help to verify the accuracy of extrapolated energy levels in the line list.

2.4.2 PS

Again the PEC was fitted using an EMO. Values of r_e and D_e were kept fixed to their spectroscopic values, $r_e = 1.89775 \text{ \AA}$ and $D_e = 37004 \text{ cm}^{-1}$. The *ab initio* PEC and SOC curves for the ground state of PS were used as the starting point in the fits.

The experimental set for the fits comprised of the $\nu = 0-9$ energies from Jenouvrier & Pascat (1978), and the reconstructed energies from PGOPHER for J up to 39.5. Although the experimental data was limited, DUO is able to extrapolate energies to higher values for the ν and J quantum numbers. The empirical PEC is compared with the *ab initio* one in Fig. 1.

Morphing was used to refine the SOC. The experimental value for r_e was used as the reference expansion point. t_∞ represents the asymptote for the morphing function ($r \rightarrow \infty$), and it equals unity in this case (Patrascu et al. 2014). Two morphing expansion parameters, A_0 and A_1 , were included in the fit because the Obs. – Calc. was reduced even further; however, no significant changes were made when fitting to the expansion parameters for $n > 1$.

Residues of the fit (Obs. – Calc.) for both molecules are plotted in Fig. 7 for all the data used in the fitting except for the less accurate vibrational energies of Verma & Singhal (1975) and Jenouvrier & Pascat (1978), which are collected in Table 2. The residuals build distinct vibronic ν, Ω patterns and diverge somewhat at higher J indicating a deficiency in our model. One of the possible sources of error is the Λ -factor for Π states, which, when properly modelled, should originate from the electronic angular momentum coupling

Table 2. Obs. – Calc. residuals for PO and PS vibrational term values in cm^{-1} . The experimentally derived energies of PO and PS are from Verma & Singhal (1975) and Jenouvrier & Pascat (1978), respectively.

ν	PO			PS		
	Obs.	Calc.	Obs. – Calc	Obs.	Calc.	Obs. – Calc
1	1220.161	1220.216	–0.055	1461.7	1461.4	0.3
2	2427.31	2427.291	0.019	2183.4	2183.2	0.2
3	3621.29	3621.242	0.04	2899.0	2899.0	0.0
4	4802.12	4802.078	0.04	3608.9	3608.8	0.1
5	5969.84	5969.799	0.04	4312.3	4312.6	–0.3
6	7124.41	7124.398	0.01	5010.2	5010.2	0.0
7	8265.85	8265.865	–0.01	5701.8	5701.7	0.1
8	9394.14	9394.184	–0.04			
9	10509.30	10509.33	–0.03			
10	11611.30	11611.29	0.01			
11	12700.05	12700.03	0.02			

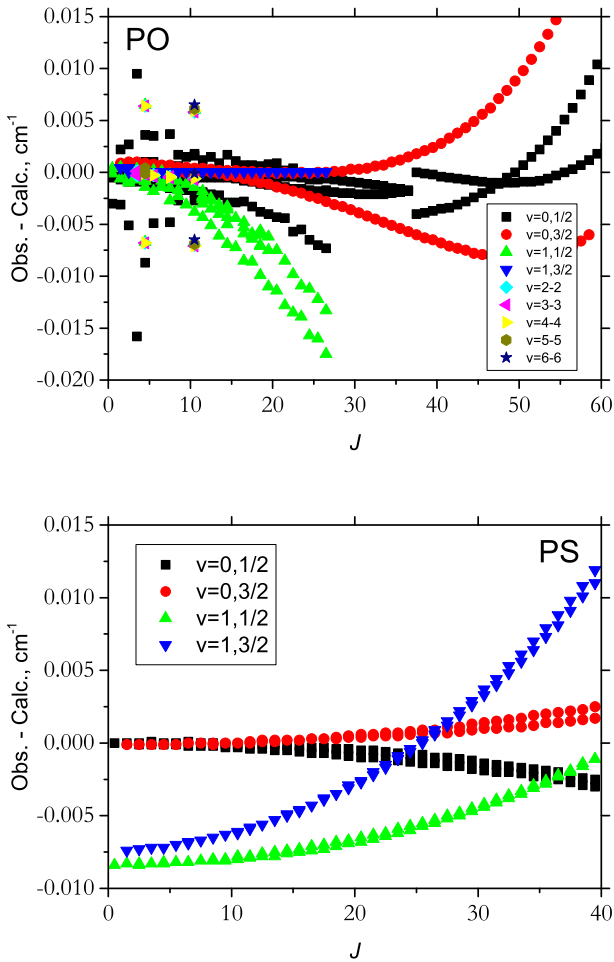


Figure 7. Observed minus Calculated (cm^{-1}) PO and PS energy term levels and line positions after refinement. The discontinuity in the PS comparison is probably because the CDMS data switch from three to two hyperfine components at $J = 36.5$, which we average to one hyperfine-free value.

to Σ states (Brown & Merer 1979). The majority of the points are situated near the zero line.

The RMS error of the fit was 0.026 cm^{-1} for all 316 experimental energies and 0.006 cm^{-1} excluding the lower accuracy vibrational data of Jenouvrier & Pascat (1978).

Table 3. Statistics for line lists for PO and PS.

	PO	PS
States (ν_{max})	$X(69)$	$X(82), B(35), a(58)$
J_{max}	234.5	320.5
ν_{max} (cm^{-1})	12 000	37 000
E'_{max} (cm^{-1})	49 000	37 000
E''_{max} (cm^{-1})	37 000	25 000
Number of energies	43 148	225 997
Number of lines	2096 289	30 394 544

For PS we have decided to include the two lowest excited electronic states $a^4\Pi$ and $B^2\Pi$ by using the corresponding *ab initio* MRCI+Q–*r*/aug-cc-pV5Z curves. In order not to destroy the accuracy of the refined model of the ground electronic state of PS, we omitted the couplings between these two states with the X state. The $B^2\Pi$ state PEC was refined by fitting to $J = 0.5$ and $J = 1.5$ rovibronic energies of this state, which we derived using parameters (T_v , r_e and B_v) of Jenouvrier & Pascat (1978) (RMS error is 0.41 cm^{-1}).

3 LINE LIST CALCULATIONS

3.1 PO (X) and PS (X, B, a) line lists

Line lists generated using DUO are comprised of a states file and a transitions file, with extensions .states and .trans, respectively (Tennyson et al. 2016c). The .states file includes the running number n , energy term values (cm^{-1}), total statistical weight, lifetime (Tennyson et al. 2016a), g -Landé factors (Semenov, Yurchenko & Tennyson 2017) and corresponding quantum numbers. The .trans file contains running numbers for the upper and lower levels, as well as the Einstein- A coefficients (Yurchenko et al. 2016).

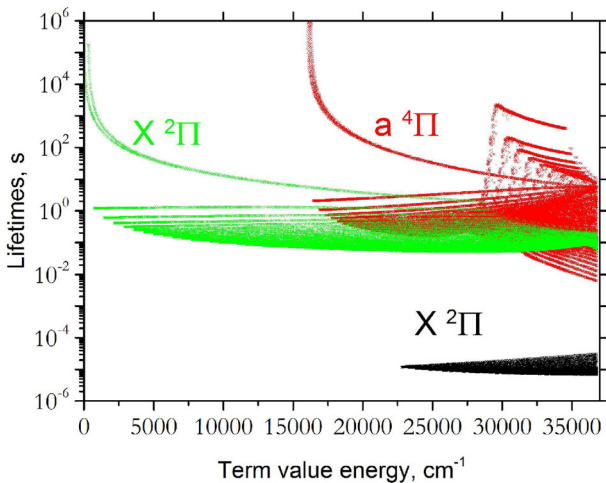
The maximum vibrational and rotational quantum numbers, ν_{max} and J_{max} are identified using the dissociation energy, D_0 . These numbers are given for both PO and PS in Table 3. The DUO integration range was chosen as $r = [0.7, 4.0] \text{ \AA}$ for PO and $r = [1.2, 4.0] \text{ \AA}$ for PS, and the respective grids comprised 501 points in conjunction with the Discrete Variable Representation (DVR) sinc method. The PO line list includes the electronic state $X^2\Pi$, while the PS line list consists of transitions between the lowest three electronic states of $X^2\Pi$, $B^2\Pi$ and $a^4\Pi$. To reduce the size of the line list, for PS the lower state energy threshold is reduced to $25\,000 \text{ cm}^{-1}$, which should cover all thermal populations much higher than 5000 K.

Table 4. Extract from the .states file for $^{31}\text{P}^{32}\text{S}$.

n	\tilde{E}	g_{tot}	J	τ	g -Landé	+ / -	e/f	State	ν	Λ	Σ	Ω
1	0.000000	4	0.5	inf	-0.000767	+	e	X2Pi	0	1	-0.5	0.5
2	733.657367	4	0.5	1.2003E+00	-0.000767	+	e	X2Pi	1	1	-0.5	0.5
3	1461.408539	4	0.5	6.0697E-01	-0.000767	+	e	X2Pi	2	1	-0.5	0.5
4	2183.215742	4	0.5	4.0934E-01	-0.000767	+	e	X2Pi	3	1	-0.5	0.5
5	2899.040733	4	0.5	3.1065E-01	-0.000767	+	e	X2Pi	4	1	-0.5	0.5
6	3608.844801	4	0.5	2.5151E-01	-0.000767	+	e	X2Pi	5	1	-0.5	0.5
7	4312.588793	4	0.5	2.1216E-01	-0.000767	+	e	X2Pi	6	1	-0.5	0.5
8	5010.233137	4	0.5	1.8413E-01	-0.000767	+	e	X2Pi	7	1	-0.5	0.5
9	5701.737858	4	0.5	1.6315E-01	-0.000767	+	e	X2Pi	8	1	-0.5	0.5
10	6387.062584	4	0.5	1.4689E-01	-0.000767	+	e	X2Pi	9	1	-0.5	0.5
11	7066.166547	4	0.5	1.3393E-01	-0.000767	+	e	X2Pi	10	1	-0.5	0.5
12	7739.008581	4	0.5	1.2337E-01	-0.000767	+	e	X2Pi	11	1	-0.5	0.5
13	8405.547119	4	0.5	1.1461E-01	-0.000767	+	e	X2Pi	12	1	-0.5	0.5
14	9065.740185	4	0.5	1.0724E-01	-0.000767	+	e	X2Pi	13	1	-0.5	0.5
15	9719.545397	4	0.5	1.0095E-01	-0.000767	+	e	X2Pi	14	1	-0.5	0.5
16	10366.919955	4	0.5	9.5535E-02	-0.000767	+	e	X2Pi	15	1	-0.5	0.5

Column	Notation
1	n
2	\tilde{E}
3	g_{tot}
4	J
5	τ
6	g
7	+ / -
8	e/f
9	State
10	ν
11	Λ
12	Σ
13	Ω

1	n	Energy level reference number (row)
2	\tilde{E}	Term value (in cm^{-1})
3	g_{tot}	Total degeneracy = $g_{\text{ns}}J(J+1)$ with $g_{\text{ns}} = 2$
4	J	Rotational quantum number
5	τ	Radiative lifetime (s)
6	g	Landé factors
7	+ / -	Total parity
8	e/f	Rotationless parity
9	State	Electronic state
10	ν	State vibrational quantum number
11	Λ	Projection of the electronic angular momentum
12	Σ	Projection of the electronic spin
13	Ω	$\Omega = \Lambda + \Sigma$ (projection of the total angular momentum)

**Figure 8.** Lifetimes of the three lower electronic states of PS computed using the PS line list.

As an additional safeguard against enhanced intensities for high overtones resulting from numerical noise, we follow the procedure used by Wong et al. (2017) and use a dipole moment threshold of 10^{-8} D.

Lifetimes for PS molecule were computed using an extended line list covering all transitions with the lower/upper state energies below 37000 cm^{-1} . They are shown in Fig. 8.

Table 5. Extract of the first 15 lines from the PS .trans file. It contains the identification numbers f and i for upper (final) and lower (initial) levels, respectively, Einstein-A coefficients denoted by A (s^{-1}) and transition frequencies ν (cm^{-1}).

i	f	A	ν
98 398	98 831	5.1886E-17	0.012 535
97 958	97 524	4.6732E-17	0.012 571
101 886	102 318	7.6872E-17	0.012 588
103 188	102 758	8.6033E-17	0.012 611
100 140	100 573	6.2520E-17	0.012 617
99 701	99 268	5.6651E-17	0.012 627
101 445	101 012	6.8893E-17	0.012 630
98 396	98 829	5.1177E-17	0.012 655
101 884	102 316	7.5904E-17	0.012 672
103 186	102 756	8.4859E-17	0.012 678
97 956	97 522	4.6028E-17	0.012 698
100 138	100 571	6.1750E-17	0.012 726
101 443	101 010	6.8055E-17	0.012 730

Table 3 summarizes the statistics for our PO and PS line lists. Extracts from the .states and .trans files for PS are given in Tables 4 and 5, respectively. Full tables for both PO and PS are available at <http://cdsarc.u-strasbg.fr/pub/cats/J/MNRAS/xxx/yy> or <http://cdsarc.u-strasbg.fr/viz-bin/qcat?J/MNRAS/xxx/yy>, as well as the ExoMol website, www.exomol.com. Note that the states files include lifetime for each individual state (Tennyson et al. 2016a); these can be useful for a variety of issues including determining critical densities.

Table 6. Comparison of calculated partition function $Q(T)$ with those of Sauval & Tatum (1984), Irwin (1981), Barklem & Collet (2016)^a and JPL (Pickett et al. 1998).

	T	This work	Irwin	Sauval & Tatum	Barklem & Collet	JPL
PO	300	1544.45		2094.29	2303.22	1539.8440
	1000	7986.52	7987.18	9182.62	9269.00	
	2000	24 522.37	24 517.88	26 386.24	26 532.2	
	3000	50 383.83	50 326.68	52 435.51	53 203.8	
	4000	86 046.26	85 818.70	88 045.63	89 775.2	
	5000	132 015.51	131 377.58	133 966.53	136 893.4	
PS	300	3525.47		3381.35	3532.94	3522.0557
	1000	23 627.9		23 710.1	23 602.8	
	2000	83 950.66		82 351.29	83 383.6	
	3000	183 804.33		177 908.26	181 066.8	
	4000	329 835.22		313 112.07	318 202	
	5000	538 812.55		490 668.67	497 144	

^aPartition function values from Sauval & Tatum (1984), Irwin (1981) and Barklem & Collet (2016) are doubled to allow for nuclear spin degeneracy and to bring them into line with the convention used here and by the other cited sources.

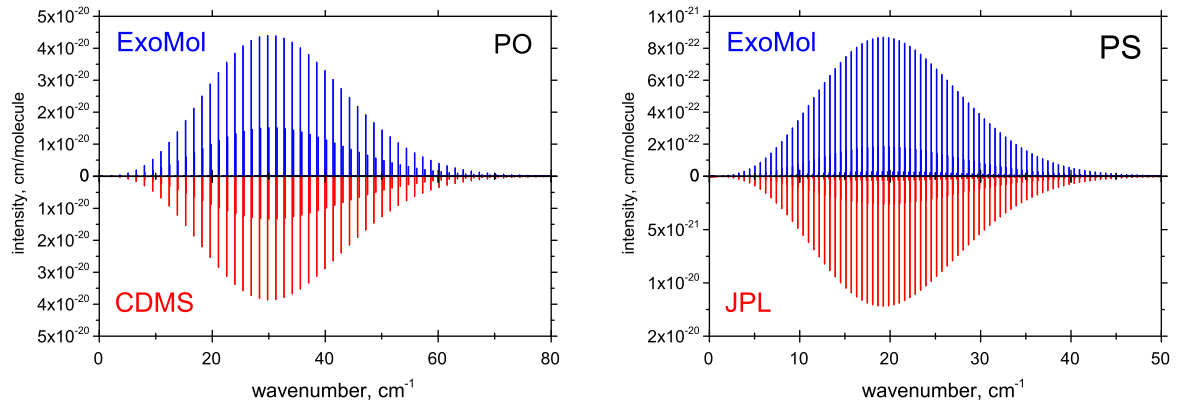


Figure 9. Comparison of pure PO (left) and PS (right) rotational lines ($T = 298$ K) with those given in CDMS (Müller et al. 2005) and JPL (Pickett et al. 1998) data bases, respectively.

3.2 Partition functions

Partition functions, $Q(T)$, for $^{31}\text{P}^{16}\text{O}$ and $^{31}\text{P}^{32}\text{S}$ were computed using the program EXOCROSS (Yurchenko et al. 2017), which was also used to calculate absorption and emission cross-sections. The nuclear statistical weight of both species is $g_{\text{ns}} = 2$. The maximum temperature was set to 5000 K and partition functions were determined in increments of 1 K. Table 6 gives partition function values at selected temperatures and a comparison with various studies. The full tabulation is given in the supplementary material.

For PO, our partition function is in good agreement with that of Irwin (1981) but agrees less well with Sauval & Tatum (1984) or the recent one of Barklem & Collet (2016), whose values appear to be too high. For PS, the agreement with Barklem & Collet (2016) is altogether more satisfactory, although their values become a little too low at the higher energies.

The partition functions from this study were represented by the series expansion following the recommendation of Vidler & Tennyson (2000):

$$\log_{10}(Q) = \sum_{i=0}^8 a_i (\log_{10}(T))^i. \quad (8)$$

The nine expansion coefficients denoted by a_i are collected as part of the supplementary material. The fits are valid for temperatures up to 5000 K.

4 RESULTS

4.1 PO $X^2\Pi$ state

Fig. 9 gives a comparison of our pure rotational spectrum with that given by CDMS (Müller et al. 2005) at $T = 298$ K. Hyperfine lines given in CDMS have been convolved for the comparison. The two spectra are in excellent agreement apart from a small difference in line intensities. This slight discrepancy arises from different values for the dipole moment: CDMS used the experimental equilibrium value 1.88 D by Kanata et al. (1988), while our *ab initio* dipole is 1.998 D at r_e .

Fig. 10 shows our predicted, temperature-dependent absorption spectrum for PO.

4.2 PS $X^2\Pi$ state

Fig. 9 shows a comparison of the rotational spectrum ($T = 298$ K) of PS simulated using our line list with that from the JPL data base (Pickett et al. 1998). The latter is also a simulated spectrum where a

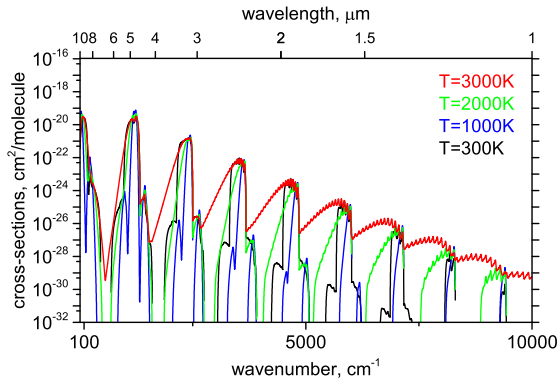


Figure 10. PO absorption spectrum at $T = 300$ (bottom), 1000, 2000 and 3000 (top) K, presented with cross-sections on a logarithmic scale. A Gaussian profile with a Half Width at Half Maximum (HWHM) = 10 cm^{-1} was used.

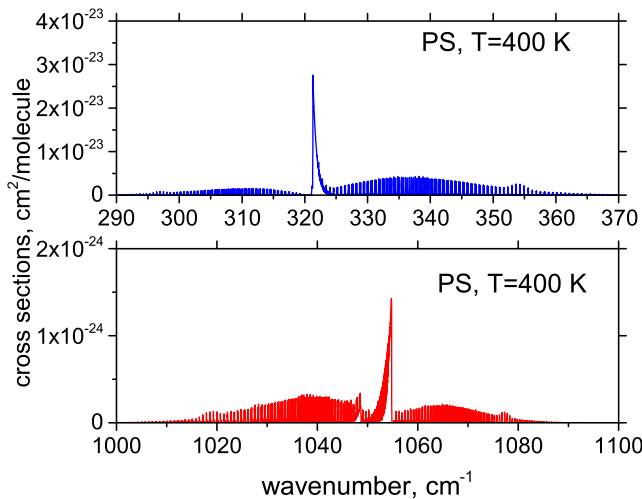


Figure 11. The Q -branches in the pure rotational and fundamental absorption bands of PS at $T = 400 \text{ K}$. A Gaussian profile with HWHM of 0.02 cm^{-1} was used.

generic dipole value of 2 D was used; therefore, the JPL's intensity scale is arbitrary. We recommend that JPL's intensities are rescaled using value for the dipole.

The Q -branches from pure rotational and fundamental bands are illustrated in Fig. 11, where the absorption spectra of PS at

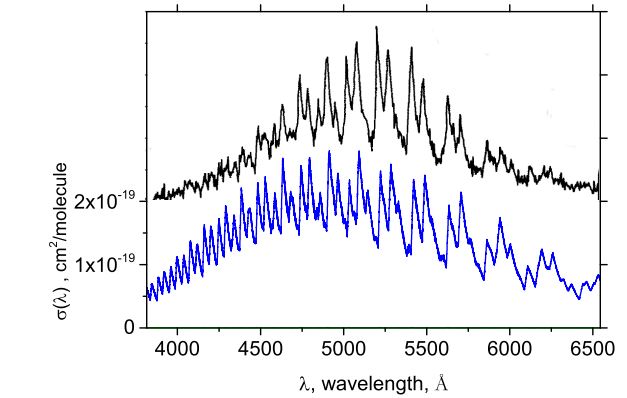
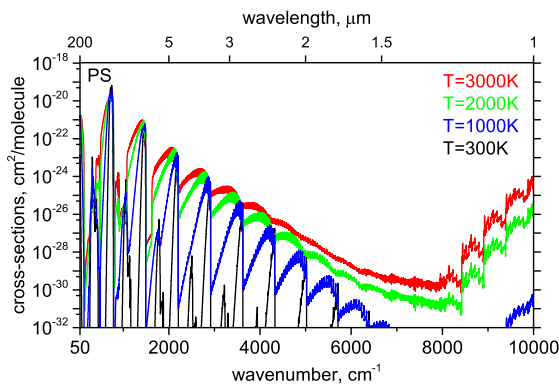


Figure 13. Predicted $B-X$ emission spectrum of PS at $T = 2000 \text{ K}$ (lower curve) with a Gaussian profile with HWHM = 50 cm^{-1} , compared to PS chemiluminescence from the reaction $\text{Cs} + \text{PSCl}_3$ by Lin et al. (1987) (upper curve). The cross-section scale refers to our computed values only.

$T = 400 \text{ K}$ are shown. These sharp features are important to astronomers because they are easily identifiable; however, the transitions themselves are relatively weak.

Fig. 12 displays the temperature-dependent absorption spectrum of PS. The spectra are prominent in the infrared as expected for rovibrational transitions within the ground electronic state. The fundamental band ($\nu = 1 \leftarrow 0$) at about $13.6 \mu\text{m}$ corresponds to the highest peak in the spectra ($\sim 1 \times 10^{-19} \text{ cm}^2 \text{ molecule}^{-1}$). The vibrational overtones at shorter wavelengths than the fundamental band are progressively weaker.

Cross-sections were calculated for transitions corresponding to the *allowed* rovibrational transitions within the $X^2\Pi$, $a^4\Pi$ and $B^2\Pi$ terms and for $B^2\Pi-X^2\Pi$ transitions. The $B^2\Pi-X^2\Pi$ band peaks in the UV region of the electromagnetic spectrum as expected.

Our predicted temperature-dependent $B^2\Pi-X^2\Pi$ absorption spectrum is shown in Fig. 12. At low temperatures it shows sharp features in the $3000\text{--}4000 \text{ \AA}$ region. These features gradually diminish at higher temperatures. Although the $B^2\Pi-X^2\Pi$ band remains featureless at high temperatures, it could possibly be used as a tracer for PS in low-temperature astronomical environments.

Fig. 13 shows a comparison of a synthetic ($T = 2000 \text{ K}$) $B-X$ emission spectrum with a chemiluminescence spectrum from the reaction $\text{Cs} + \text{PSCl}_3$ observed by Lin et al. (1987).

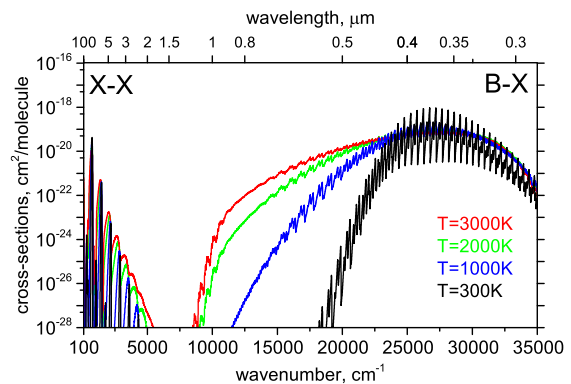


Figure 12. Absorption spectrum for the ground state of PS as a function of temperature ($T = 300, 1000, 2000$ and 3000 K). Gaussian profiles with HWHM = 1 cm^{-1} (left-hand panel) and 10 cm^{-1} (right-hand panel) were used.

5 DISCUSSION AND CONCLUSION

The new line lists for PO ($X^2\Pi$) and PS ($X^2\Pi$, $B^2\Pi$ and $a^4\Pi$) are the most comprehensive to date. The PO line list, covering the $X^2\Pi$ state, should be sufficient for modelling infrared spectra for this species at long wavelengths. The PS line list has a larger coverage, up to $37\,000\text{ cm}^{-1}$ and considers two low-lying excited electronic states, $B^2\Pi$ and $a^4\Pi$ in addition to the ground $X^2\Pi$ state. This uses the refined curves for the X and B states, but with the addition of the unrefined *ab initio* curves for the $a^4\Pi$ electronic state as relevant experimental data was unavailable. This line list is designed to aid the identification of spectral features of PS at short wavelengths, although a more accurate line list will be necessary for a full spectral analysis. Our line list shows a strong banded structure for absorption at 300 K in the 3500 \AA region. However, at higher temperatures the absorption becomes a very broad feature with little to no structure suggesting that observation of the $B^2\Pi$ – $X^2\Pi$ is unlikely to be useful for detecting PS in hot environments. The Q -branch transitions from the spin–orbit split components can be used as a diagnostic for PS in observational spectra due to the characteristically sharp peak in both absorption and emission. However, the transitions themselves are relatively weak, and so sensitive detectors would be required.

It is difficult to provide specific uncertainties for theoretical calculations. However, our fits to the experimental transition frequencies give some insight into the accuracy of the line positions. For PO, this is 0.001 cm^{-1} for pure rotational transitions and 0.05 cm^{-1} for transitions involving vibrational excitation. These estimates cover the range where experimental data is available ($v \leq 11$ and $J \leq 22.5$); for values outside these ranges the uncertainty is expected to grow approximately linearly with v and quadratically with J . Comparison with the rather uncertain experimentally determined dipole suggests that our computed intensities for PO are unlikely to be accurate to better than 10 per cent, and are possibly worse than this. For PS, there is less high-quality experimental data for line positions available. For transitions within the X state, pure rotational transitions are accurate to about 0.006 cm^{-1} for $J \leq 39.5$; the accuracy of the vibrational transition frequencies is limited by a lack of high-accuracy measurements and are unlikely to good to better than 0.2 cm^{-1} . In the absence of any experimental determinations, we can only estimate the uncertainty of vibration–rotation transition intensities as being between 10 and 20 per cent. The vibronic line list for PS is considerably less accurate with transition frequencies unlikely to be better than 0.5 cm^{-1} and intensities only reliable to about ± 50 per cent.

These line lists, which we call the POPS line lists, can be downloaded from the <http://cdsarc.u-strasbg.fr> or from www.exomol.com.

So far phosphorus mononitride (PN) (Yorke et al. 2014) and phosphine (PH_3) (Sousa-Silva et al. 2015) are the only phosphorus-bearing molecules whose line lists have been computed as part of the ExoMol project. PN was the first P-bearing molecule to be astronomically observed by Turner & Bally (1987) and Ziurys (1987) in Orion KL, Sagittarius B2 and W51; PH_3 was discovered in Jupiter and Saturn from Voyager data in 1975 (Bregman, Lester & Rank 1975; Ridgway, Wallace & Smith 1976), and recently detected around the C-rich AGB star, IRC+10216 (Agúndez et al. 2008). This paper presents line lists for PO and PS. A line list for PH is currently under construction while an empirical line list for CP, which can also be downloaded from the ExoMol website, was provided by Ram et al. (2014).

ACKNOWLEDGEMENTS

This work was supported by the ERC under the Advanced Investigator Project 267219. We also acknowledge the networking support by the COST Action CM1405 MOLIM. This work made extensive use of the Legion HPC at UCL.

REFERENCES

- Agúndez M., Cernicharo J., Pardo J. R., Guélin M., Phillips T. G., 2008, *A&A*, 485, L33
- Agundez M., Cernicharo J., Decin L., Encrenaz P., Teyssier D., 2014, *ApJ*, 790, L27
- Andreazza C. M., de Almeida A. A., Borin A. C., 2016, *MNRAS*, 457, 3096
- Bailleux S., Bogey M., Demuynck C., Liu Y., Walters A., 2002, *J. Mol. Spectrosc.*, 216, 465
- Balasubramanian T. K., Dixit M. N., Narasimham N. A., 1979, *Pramana*, 12, 707
- Barklem P. S., Collet R., 2016, *A&A*, 588, A96
- Ben Yaghlane S., Francisco J. S., Hochlaf M., 2012, *J. Chem. Phys.*, 136
- Bregman J. D., Lester D. F., Rank D. M., 1975, *ApJ*, 202, L55
- Brown J. M., Merer A. J., 1979, *J. Mol. Spectrosc.*, 74, 488
- Brown J. M. et al., 1975, *J. Mol. Spectrosc.*, 55, 500
- Bruna P. J., Grein F., 1987, *J. Phys. B: At. Mol. Opt. Phys.*, 20, 5967
- Butler J. E., Kawaguchi K., Hirota E., 1983, *J. Mol. Spectrosc.*, 101, 161
- De Beck E., Kaminski T., Patel N. A., Young K. H., Gottlieb C. A., Menten K. M., Decin L., 2013, *A&A*, 558, 9
- de Brouckere G., 1999, *J. Phys. B: At. Mol. Opt. Phys.*, 32, 5415
- de Brouckere G., 2000, *Chem. Phys.*, 262, 211
- Dimur C., Pauzat F., Ellinger Y., Berthier G., 2001, *Spectra Chim. Acta A*, 57, 859
- Dressler K., Miescher E., 1955, *Proc. Nat. Acad. Sci.*, 68, 542
- Drowart J., Myers C. E., Szwarc R., Auwera-Mahieu A. V., Uy O. M., 1973, *High Temp. Sci.*, 5, 482
- Ghosh S. N., Verma R. D., 1978, *J. Mol. Spectrosc.*, 73, 266
- Huber K. P., Herzberg G., 1979, *Molecular Spectra and Molecular Structure IV. Constants of Diatomic Molecules*. Van Nostrand Reinhold Company, New York
- Irwin A. W., 1981, *ApJS*, 45, 621
- Jenouvrier A., Pascat B., 1978, *Can. J. Phys.*, 56, 1088
- Kalcher J., 2002, *Phys. Chem. Chem. Phys.*, 4, 3311
- Kanata H., Yamamoto S., Saito S., 1988, *J. Mol. Spectrosc.*, 131, 89
- Karna S. P., Grein F., 1992, *Mol. Phys.*, 77, 135
- Karna S. P., Bruna P. J., Grein F., 1988, *J. Phys. B: At. Mol. Opt. Phys.*, 21, 1303
- Kawaguchi K., Hirota E., Ohishi M., Suzuki H., Takano S., Yamamoto S., Saito S., 1988, *J. Mol. Spectrosc.*, 130, 81
- Klein H., Klich E., Winnewisser G., 1999, *Z. Naturforschung A*, 54, 137
- Lee E. G., Seto J. Y., Hirao T., Bernath P. F., Le Roy R. J., 1999, *J. Mol. Spectrosc.*, 194, 197
- Lefloch B. et al., 2016, *MNRAS*, 462, 3937
- Li Y.-L., Sun S., Chan L. S., 2013, *Ecol. Evol.*, 3, 115
- Lin K. K., Balling L. C., Wright J. J., 1987, *Chem. Phys. Lett.*, 138, 168
- Liu H., Shi D. H., Sun J. F., Zhu Z. L., 2013, *J. Quant. Spectrosc. Radiat. Transf.*, 121, 9
- Lodi L., Tennyson J., 2010, *J. Phys. B: At. Mol. Opt. Phys.*, 43, 133001
- Maciá E., Hernández M. V., Oró J., 1997, *Orig. Life Evol. Biosph.*, 27, 459
- MacKay D., Charnley S., 2001, *MNRAS*, 325, 545
- Matthews H. E., Feldman P. A., Bernath P. F., 1987, *ApJ*, 312, 358
- McKemmish L. K., Yurchenko S. N., Tennyson J., 2016, *Mol. Phys.*, 114, 3232
- Medvedev E. S., Meshkov V. V., Stoloyarov A. V., Ushakov V. G., Gordon I. E., 2016, *J. Mol. Spectrosc.*, 330, 36
- Metropoulos A., Papakondylis A., Mavridis A., 2003, *J. Chem. Phys.*, 119, 5981

- Milam S. N., Halfen D. T., Tenenbaum E. D., Apponi A. J., Woolf N. J., Ziurys L. M., 2008, *ApJ*, 684, 618
- Moussaoui Y., Ouamerli O., De Mare G. R., 1998, *J. Mol. Struct. (THEOCHEM)*, 425, 237
- Moussaoui Y., Ouamerli O., De Mare G. R., 2003, *Int. Rev. Phys. Chem.*, 22, 641
- Muller H. S. P., Woon D. E., 2013, *J. Phys. Chem. A*, 117, 13868
- Müller H. S. P., Schlöder F., Stutzki J., Winnewisser G., 2005, *J. Mol. Struct. (THEOCHEM)*, 742, 215
- Narasimham N. A., Subramanian T. K. B., 1969, *J. Mol. Spectrosc.*, 29, 294
- Narasimham N. A., Balasubramanian T. K., 1971, *J. Mol. Spectrosc.*, 37, 371
- Ohishi M. et al., 1988, *ApJ*, 329, 511
- Patrascu A. T., Hill C., Tennyson J., Yurchenko S. N., 2014, *J. Chem. Phys.*, 141, 144312
- Pickett H. M., Poynter R. L., Cohen E. A., Delitsky M. L., Pearson J. C., Müller H. S. P., 1998, *J. Quant. Spectrosc. Radiat. Transf.*, 60, 883
- Polyansky O. L., Bielska K., Ghysels M., Lodi L., Zobov N. F., Hodges J. T., Tennyson J., 2015, *Phys. Rev. Lett.*, 114, 243001
- Qian H. B., 1995, *J. Mol. Spectrosc.*, 174, 599
- Ram R. S., Brooke J. S. A., Western C. M., Bernath P. F., 2014, *J. Quant. Spectrosc. Radiat. Transf.*, 138, 107
- Rao T. V. R., Reddy R. R., Rao P. S., 1981, *Physica B & C*, 106, 445
- Ridgway S. T., Wallace L., Smith G. R., 1976, *ApJ*, 207, 1002
- Rivilla V. M., Fontani F., Beltrán M. T., Vasyunin A., Caselli P., Martín-Pintado J., Cesaroni R., 2016, *ApJ*, 826, 161
- Sauval A. J., Tatum J. B., 1984, *ApJS*, 56, 193
- Semenov M., Yurchenko S. N., Tennyson J., 2017, *J. Mol. Spectrosc.*, 330, 57
- Sousa-Silva C., Al-Refaie A. F., Tennyson J., Yurchenko S. N., 2015, *MNRAS*, 446, 2337
- Spielfiedel A., Handy N. C., 1999, *Phys. Chem. Chem. Phys.*, 1, 2401
- Sun J. F., Wang J. M., Shi D. H., 2012, *Int. J. Quantum Chem.*, 112, 672
- Šurkus A. A., Rakauskas R. J., Bolotin A. B., 1984, *Chem. Phys. Lett.*, 105, 291
- Tenenbaum E. D., Woolf N. J., Ziurys L. M., 2007, *ApJ*, 666, L29
- Tennyson J., 2012, *WIREs Comput. Mol. Sci.*, 2, 698
- Tennyson J., 2014, *J. Mol. Spectrosc.*, 298, 1
- Tennyson J., Yurchenko S. N., 2012, *MNRAS*, 425, 21
- Tennyson J., Yurchenko S. N., 2017, *Mol. Astrophys.*, 8, 1
- Tennyson J., Hulme K., Naim O. K., Yurchenko S. N., 2016a, *J. Phys. B: At. Mol. Opt. Phys.*, 49, 044002
- Tennyson J., Lodi L., McKemmish L. K., Yurchenko S. N., 2016b, *J. Phys. B: At. Mol. Opt. Phys.*, 49, 102001
- Tennyson J. et al., 2016c, *J. Mol. Spectrosc.*, 327, 73
- Tsuji T., 1973, *A&A*, 23, 411
- Turner B. E., Bally J., 1987, *ApJ*, 321, L75
- Verma R. D., Singhal S. R., 1975, *Can. J. Phys.*, 53, 411
- Vidler M., Tennyson J., 2000, *J. Chem. Phys.*, 113, 9766
- Visscher C., Lodders K., Fegley B. Jr, 2006, *ApJ*, 648, 1181
- Wang H. Q., Gu Y. S., Liu C. P., Yin Y. J., Cao D. Z., Li S. T., 1993, *Acta Chim. Sin.*, 51, 18
- Werner H.-J., Knowles P. J., Knizia G., Manby F. R., Schütz M., 2012, *WIREs Comput. Mol. Sci.*, 2, 242
- Western C. M., 2017, *J. Quant. Spectrosc. Radiat. Transf.*, 186, 221
- Wong A., Yurchenko S. N., Bernath P., Mueller H. S. P., McConkey S., Tennyson J., 2017, *MNRAS*, 470, 882
- Yamaguchi T. et al., 2011, *Publ. Astron. Soc. Jpn.*, 63, L37
- Yamaguchi T. et al., 2012, *Publ. Astron. Soc. Jpn.*, 64, 105
- Yorke L., Yurchenko S. N., Lodi L., Tennyson J., 2014, *MNRAS*, 445, 1383
- Yurchenko S. N., Lodi L., Tennyson J., Stolyarov A. V., 2016, *Comput. Phys. Commun.*, 202, 262
- Yurchenko S. N., Amundsen D. S., Tennyson J., Waldmann I. P., 2017, *A&A*
- Ziurys L. M., 1987, *ApJ*, 321, L81

SUPPORTING INFORMATION

Supplementary data are available at [MNRAS](https://www.mnras.org) online.

Please note: Oxford University Press is not responsible for the content or functionality of any supporting materials supplied by the authors. Any queries (other than missing material) should be directed to the corresponding author for the article.

This paper has been typeset from a \TeX/L\AA\TeX file prepared by the author.